arXiv:1702.05076v2 [physics.optics] 1 Mar 2017

Integrated Ultra-High-Q Optical Resonator

Ki Youl Yang[1]*, Dong Yoon Oh[1]*, Seung Hoon Lee[1]*, Qi-Fan Yang[1], Xu Yi[1] and Kerry Vahala[1†]
[1]T. J. Watson Laboratory of Applied Physics, California Institute of Technology, Pasadena, California 91125, USA.
*These authors contributed equally to this work.
[†]Corresponding author: vahala@caltech.edu

Optical microcavities[1] are compact, often chip-based devices, that are essential in technologies spanning frequency metrology[2,3] to biosensing[4–6]. They have also enabled new science in quantum information[7] and cavity optomechanics[8]. Performance requirements in subjects like cavity-QED and sensing have long placed emphasis on low-optical-loss (high-Q-factor) micrometer-scale resonators. However, an array of system-on-a-chip applications have emerged that also require millimeter-scale devices. To avoid impractically-high pumping powers associated with the increased stored energy of these larger devices, Q factors well above those possible in existing integrable resonators are needed. Here, we demonstrate a silicon-chip-based microcavity that combines high-Q performance with monolithic integration. Q factors over 200 million are achieved, and an integrable soliton microcomb having a detectable repetition rate is demonstrated. The device represents a critical advance that can be used in newly proposed miniature optical-synthesizers[9], secondary time standards[10] and compact spectroscopy systems[11], all of which require detectable-rate integrable microcombs. Moreover, nascent chip-based optical inertial sensor systems[12], which have recently achieved navigation-grade sensitivity[13], require high-Q, large mode volume designs to attain high Sagnac rotation sensitivity. Therefore, the device reported here also provides a pathway to high sensitivity at low operating power in a fully-integrated rotation sensor.

Optical microcavities provide diverse functions that include frequency microcombs[2,14], soliton mode-locked microcombs[15,16], high-coherence Brillouin lasers[17], bio and nano-particle sensors[4–6], cavity optomechanical systems[8], parametric oscillators[18,19], Raman lasers[20], and strong-coupling cavity QED systems[21]. Key performance metrics scale at least as $1/Q$ and frequently as $1/Q^2$ across all applications areas[1] and have accounted for a sustained period of progress in boosting Q factor by reducing optical loss in micro- and milli-scale resonators. Numerous cavity designs routinely exceed a Q factor of 100 million and higher[1,17,22,23]. Also, advances in resonator integration have made possible on-chip waveguide coupling to low-optical-loss resonators using silicon nitride and other materials[24–29]. Octave-span, THz-repetition-rate, soliton combs with integrated waveguides have resulted from these new capabilities[30,31]. Nonetheless, finding a fabrication pathway that maximizes Q factor while maintaining a scalable, integration-ready fabrication process has proven challenging. Fiber tapers[32,33] and prisms[19] are used, for example, to efficiently couple power to the highest Q, silica and crystalline-based devices.

At the same time, proposals for miniature navigation, remote sensing and metrology systems have emerged requiring the performance advantages of higher-Q silica and crystalline designs, but with full integration capability. These new application areas also require millimeter-scale resonators. For example, detectable pulse repetition rates are needed in frequency combs in order to self-reference the comb[34]. However, to attain detectable rates in a microcavity frequency comb the mode volume must be substantially increased to reduce the resonator free-spectral-range (FSR)[35]. Similarly, optical gyroscopes need large diameter resonators to increase the Sagnac effect and boost sensitivity. For example, recent Brillouin-based gyroscopes use an 18 mm diameter disk-laser design to achieve navigation-level sensitivity[13]. Stronger resonant build-up provided by higher-Q devices is necessary in each of these applications in order to sustain a higher resulting stored energy at an acceptable pump power level. Presently, only taper and prism coupled crystalline and silica resonators are used.

In this work, a monolithic microcavity featuring both a Q factor greater than 200 million and an integrated waveguide is demonstrated. The resonator is based on a novel silica ridge fabrication process and the waveguide is composed of plasma-enhanced chemical-vapor-deposited (PECVD) silicon nitride. The structure is fabricated on a silicon wafer using only standard lithography, wet etch, and dry etch steps. The materials, process steps and, in particular, the PECVD silicon nitride waveguide are compatible with other photonic devices. As a result, this process enables full integration of ultra-high-Q devices with other photonic devices on a silicon wafer.

A cross-sectional rendering of the resonator structure is shown in Fig. 1a. A mode field is also included. In Fig. 1b, a scanning electron microscope (SEM) image shows three ridge resonators connected by a common silicon nitride waveguide (false color red in the image). White arrows indicate how light guided in the silicon nitride couples into the ridge resonator where it circulates and then recouples to the waveguide. Details on the fabrication process are provided in the Methods Section. The ridge resonator is composed of thermal silica and has a

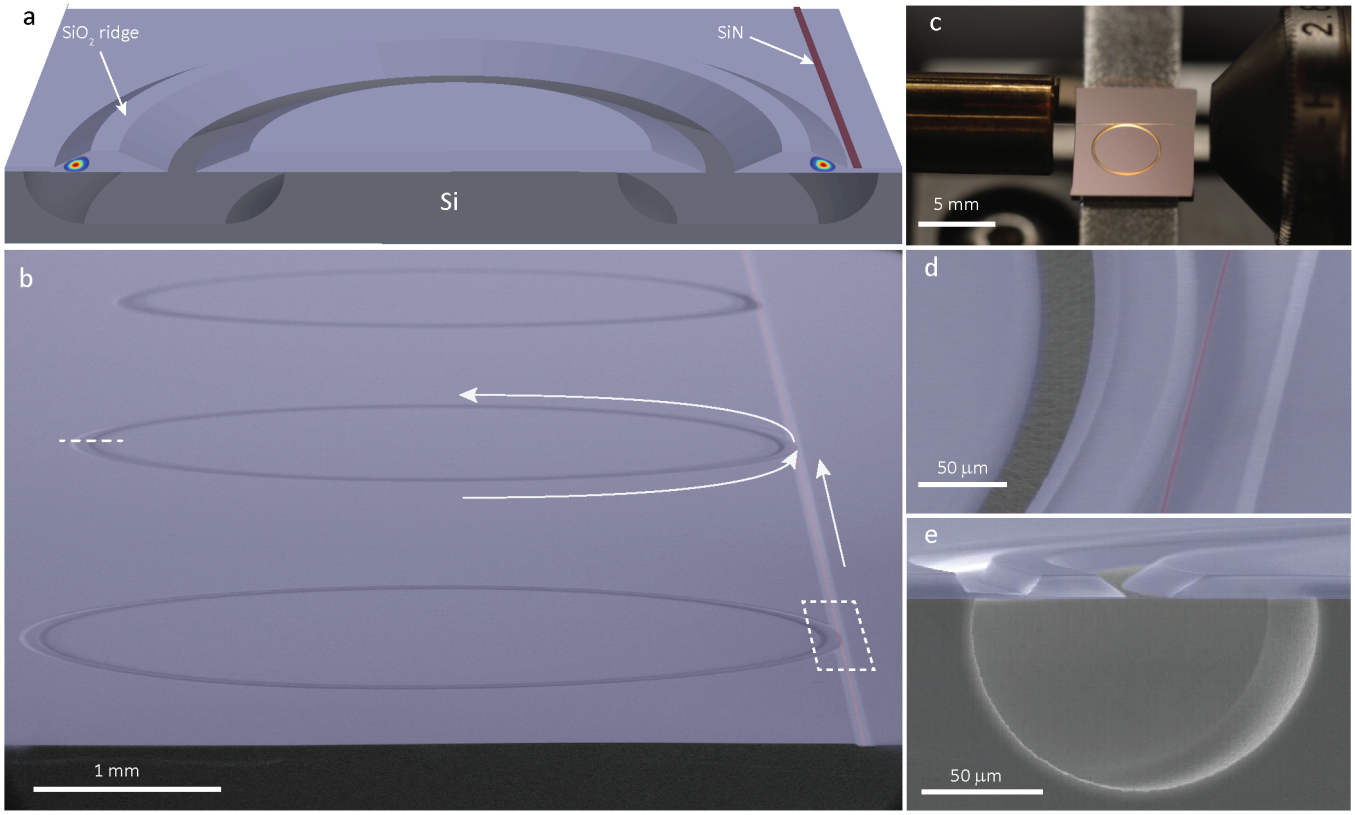

FIG. 1: **Integrated ultra-high-Q microresonator** (**a**) Rendering showing silica ridge resonator with nearby silicon nitride waveguide. Fundamental spatial mode is illustrated in color. (**b**) SEM image of three ridge resonators with a common silicon nitride waveguide (false red color). White arrows show the direction of circulation within the center resonator for the corresponding direction of coupling from the waveguide. Dashed white box is the region for the zoom-in image in 1d. Dashed white line segment gives the location of cleavage plane used for preparation of the SEM image in 1e. (**c**) Photograph of a single resonator with endfire coupling provided by a lensed fiber (left) and aspheric lens (right). (**d**) SEM zoom-in image of the waveguide-resonator coupling region shown within the dashed white box in 1b. (**e**) SEM image of resonator cross section prepared by cleaving at the dashed white line in 1b.

maximum thickness of approximately 8.5 microns. The silicon nitride waveguide has a thickness of approximately 250 nm. It is initially 3 to 3.5 microns in width at the edge of the wafer and is tapered to about 900 nm near the resonator so as to phase match to the resonator optical mode. The lightwave evanescently couples between the silicon nitride waveguide and the microcavity through the silica layer which supports the waveguide. Shown in Fig. 1c is a photograph of end-fire coupling to a single resonator using a lensed fiber (left) and light collection with an aspheric lens (right). Approximately 25 % of the power could be coupled from the lensed optical fiber to the silicon nitride waveguide. No attempt to improve coupling was made, but in the future a tapered waveguide end can be introduced to improve the coupling efficiency[36]. SEM zoom-in and cross-sectional views are shown in Fig. 1d and in Fig. 1e.

Spectral measurements of the integrated microcavity were performed by end-fire coupling to a tunable external cavity laser and monitoring of the transmission through the waveguide-coupled device as the laser is scanned (Fig. 1c). The devices tested had a FSR of approximately 15 GHz (ridge ring diameter of approximately 4.3 mm). Fig. 2a presents a spectral scan containing over two FSRs. Several transverse modes appear in the scan. These transverse mode families were identified by collecting broad dispersion curves for the resonator modes as described below and comparing to numerical modeling. High-resolution scans of the TE1 and TM1 modes are presented in Fig. 2b. The frequency scales in the scans are calibrated using a fiber Mach-Zehnder interferometer which appears as the green sinusoid at the lower half of each panel. Spectral calibration of the interferometer is performed using microwave sidebands generated by phase modulation of the laser. A linewidth fitting algorithm gives an intrinsic Q factor of 120 million for the TE1 mode and 207 million for the TM1 mode. To further confirm the high optical Q factor of the TM1 mode, cavity ring down was performed[37]. A superposition of ten ring-down traces is presented in Fig. 2c and gives an intrinsic Q factor of 214 million in close agreement with the linewidth data.

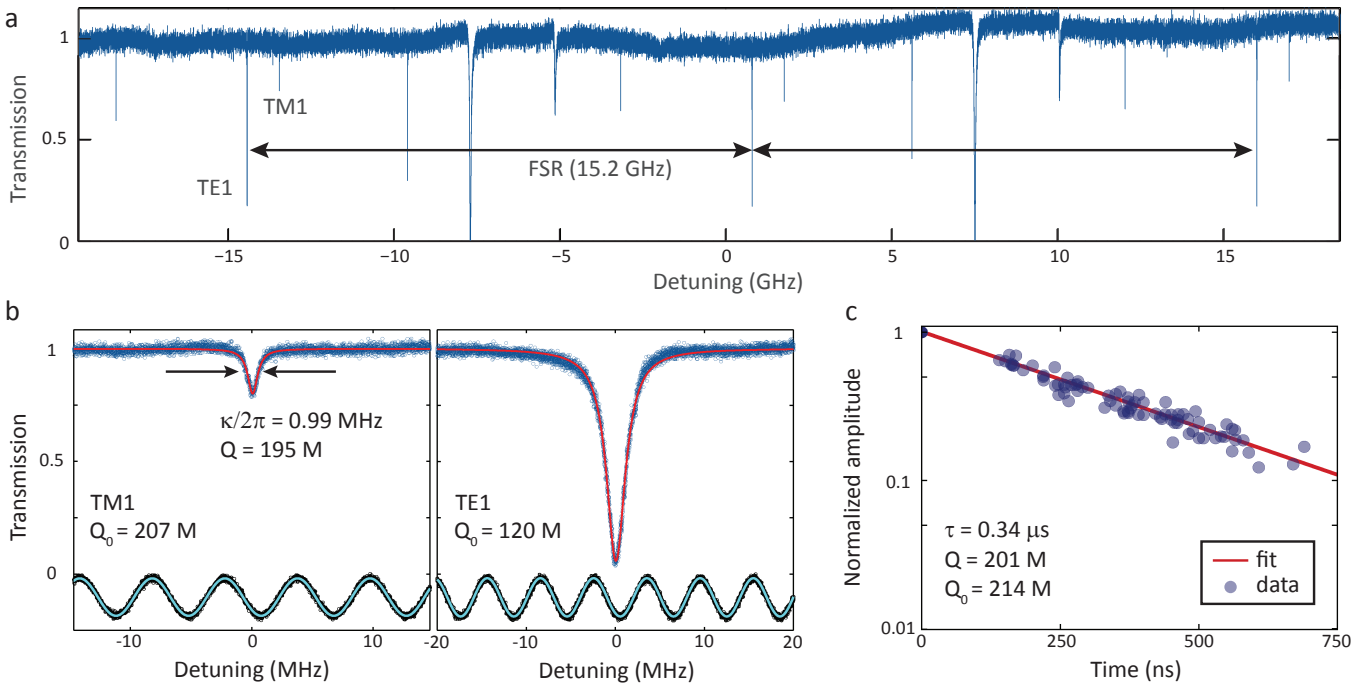

FIG. 2: **Spectral scan of integrated ridge resonator and ring-down measurement** (**a**) Spectral scan encompassing two free-spectral-ranges. (**b**) High resolution zoom-in scan for the TM1 and TE1 modes with intrinsic (Q_o) and loaded (Q) quality factors, as well as the linewidth ($\kappa/2\pi$) indicated (M = million). The green sinusoidal signal is a frequency calibration scan using a radio-frequency calibrated fiber Mach-Zehnder interferometer (free-spectral range is 5.979 MHz). (**c**) Superposition of 10 cavity-ringdown signal scans for the TM1 mode with the corresponding decay time and the loaded and intrinsic Q factors.

Dissipative Kerr solitons represent a major advance in the subject of frequency microcombs[15]. They provide highly reproducible optical spectra, have achieved 2/3 and full octave span coverage[31,38] and exhibit highly stable repetition rates[16]. Importantly, these devices provide a miniature platform for potential full integration of frequency comb systems. However, as noted above, a detectable repetition rate soliton comb using an integrable device platform has not yet been realized. Therefore, as a demonstration of the new performance capability provided by the integrated ridge resonator, a 15 GHz soliton stream was generated.

The TE1 mode family dispersion was first characterized by measuring the frequency of all modes between 1530 nm and 1580 nm using an external cavity laser calibrated by the Mach-Zehnder interferometer described above. This data was then plotted by removing both an offset frequency (ω_0) and a linear dispersion term proportional to the FSR (D_1) of the TE1 mode family at ω_0 ($D_1/2\pi$ = 15.2 GHz was measured). Modes are indexed using the label μ with $\mu = 0$ assigned to the mode at frequency ω_0, which is also the mode that is pumped to generate the solitons. The resulting data are plotted in Fig. 3a. The red curve is a parabola showing that the mode family is dominated by second-order dispersion over the range of modes measured. A fitting gives $D_2/2\pi = 6.4$ kHz where $\omega_\mu = \omega_0 + D_1\mu + D_2\mu^2/2$. Significantly, there is no observable mode-crossing-induced distortion of the mode family, therefore making the mode family well suited for soliton formation[15,16]. Solitons were triggered and stabilized using the power kick[38] and capture-lock technique[39]. An optical spectrum is shown for a single soliton state in Fig. 3b. Visible in the spectrum is the optical pump wave. To confirm the detectable repetition rate, the soliton pulse stream was directly detected and analyzed on an electrical spectrum analyzer. The electrical spectrum is provided as an inset to Fig. 3b and shows a measured repetition rate near 15.2 GHz. To confirm the pulse nature of the soliton the frequency resolved optical gate (FROG) method was used to measure the pulse train[15]. The FROG data is presented in Fig. 3c.

In summary, we have demonstrated a resonator having an optical Q factor greater than 200 million with a monolithically integrated waveguide. Soliton generation at 15 GHz was also demonstrated to illustrate functionality currently not attainable with other integrated resonator platforms. The waveguide material, PECVD silicon nitride, is among the most widely used waveguide materials in the photonics industry and provides a nearly universal interface to other photonic devices fabricated on a common silicon wafer. In addition to the detectable repetition rate soliton microcomb, high-coherence Brillouin lasers and Brillouin gyroscopes should be readily

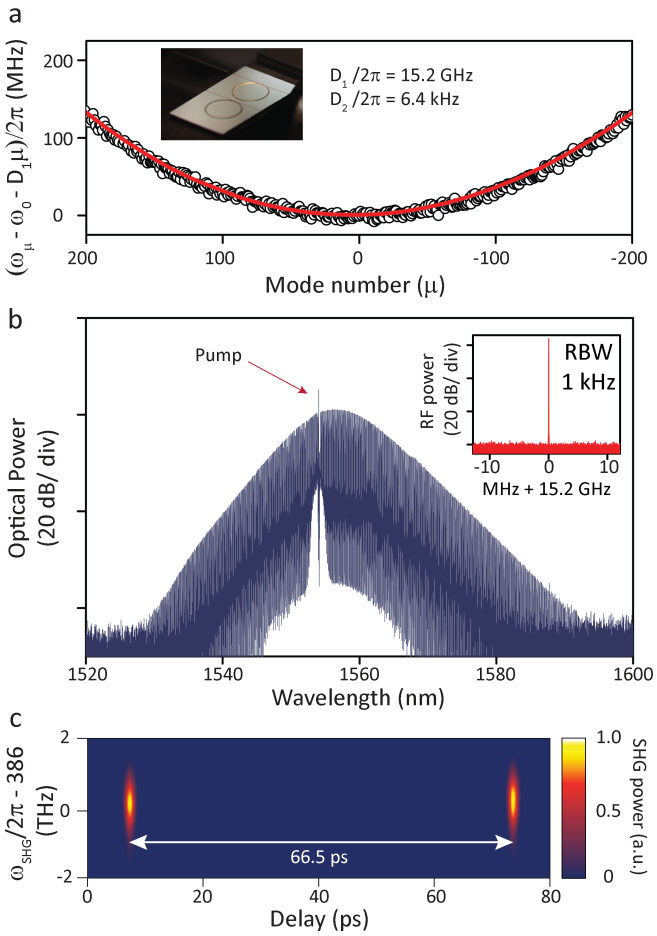

FIG. 3: **Demonstration of detectable repetition rate temporal solitons in an integrated optical microresonator** (**a**) Measured mode frequencies plotted versus mode number for the TE1 mode family with linear dispersion removed. The red curve is a parabola showing that the dispersion is primarily second order over 400 modes. Legend gives the free-spectral range (D_1) for mode $\mu = 0$ and the second-order dispersion (D_2). The inset is a photograph of two ridge resonators. (**b**) Optical spectrum of soliton with pump line indicated. Inset shows the electrical spectrum of the detected soliton pulse stream (RBW: resolution bandwidth) (**c**) FROG scan of single soliton state in 3b showing the single pulse signal with pulse period of 66.5 ps corresponding to resonator round-trip time.

transferrable to the process demonstrated here.

Methods Referring to Fig. 4, the fabrication process begins by growing a thermal silica layer on a high-purity float-zone silicon wafer. This layer is then patterned and wet etched using buffered hydrofluoric acid (HF) according to a process used to create wedge resonators[17]. The resulting etched oxide forms a circular disk structure that defines the exterior of the resonator. A subsequent thermal oxidation grows the oxide layer beneath the oxide disk. This growth is followed by deposition of 500 nm of PECVD silicon nitride. Lithography and a shallow ICP RIE dry-etch steps are then applied to partially etch the silicon nitride. Phosphoric acid is used to fully define the silicon nitride waveguide. A thin layer (20 nm) of silica is applied by atomic layer deposition to protect the silicon nitride waveguide during the final dry etch step below. A lithography/wet-etch step is then used to open an interior, ring aperture to the silicon substrate. In the final step, xenon difluoride (XeF_2) etches the silicon through the interior ring aperture so as to create an optical cavity.

Acknowledgment The authors thank Oskar Painter and Barry Baker for assistance with the PECVD silicon nitride process, Harry Atwater and Seyoon Kim for assistance with silica atomic layer deposition, and Matthew Hunt for assistance with electron beam microscopy. The authors gratefully acknowledge the Defense Advanced Research Projects Agency under the DODOS program (Award No. HR0011-15-C-0055, Sub Award KK1540) and the Kavli Nanoscience Institute.

Author contributions KYY, DYO, SHL and KV conceived the fabrication process and resonator design. KYY, DYO and SHL fabricated and tested the resonator structures. KYY, DYO and SHL conducted soliton measurement with assistance from QFY and XY. All authors analyzed the data and contributed to writing the manuscript.

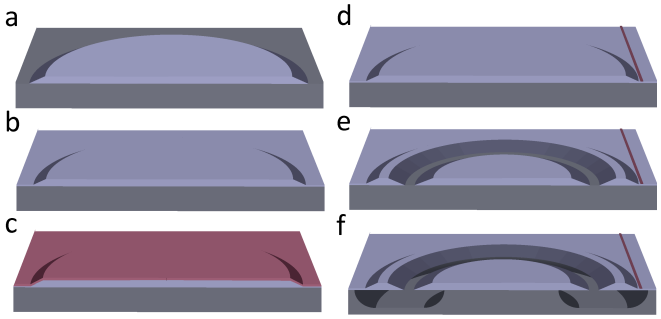

FIG. 4: **Fabrication process for integrated ultra-high-Q microresonator** (**a**) Silica disk is defined on silicon by photolithography and HF etching of an initial silica layer. (**b**) Thermal oxidation grows a second oxide layer beneath the etched silica disk. (**c**) PECVD silicon nitride is deposited. (**d**) Silicon nitride waveguide is defined on silica layer by lithography and etching. (**e**) Lithography and wet etch of the silica defines a ring aperture to the silicon substrate. (**f**) XeF_2 etches the silicon through the ring aperture (also see Fig. 1a).

[1] Vahala, K. J. Optical microcavities. *Nature* **424**, 839–846 (2003).

[2] Kippenberg, T. J., Holzwarth, R. & Diddams, S. A. Microresonator-based optical frequency combs. *Science* **332**, 555–559 (2011).

[3] Papp, S. B. *et al.* Microresonator frequency comb optical clock. *Optica* **1**, 10–14 (2014).

[4] Vollmer, F. & Arnold, S. Whispering-gallery-mode biosensing: label-free detection down to single molecules. *Nature Methods* **5**, 591–596 (2008).

[5] Lu, T. *et al.* High sensitivity nanoparticle detection using optical microcavities. *Proceedings of the National Academy of Sciences* **108**, 5976–5979 (2011).

[6] Vollmer, F. & Yang, L. Label-free detection with high-Q microcavities: a review of biosensing mechanisms for integrated devices. *Nanophotonics* **1**, 267–291 (2012).

[7] Kimble, H. J. The quantum internet. *Nature* **453**, 1023–1030 (2008).

[8] Kippenberg, T. J. & Vahala, K. J. Cavity optomechanics: back-action at the mesoscale. *Science* **321**, 1172–1176 (2008).

[9] Spencer, D. T. *et al.* Towards an integrated-photonics optical-frequency synthesizer with <1 Hz residual frequency noise. In *Optical Fiber Communication Conference*, M2J.2 (2017).

[10] Frank, I. *et al.* A low-power, chip-scale optical atomic clock with enhanced stability. In *Joint Navigation Conference* (2017).

[11] Suh, M.-G., Yang, Q.-F., Yang, K. Y., Yi, X. & Vahala, K. J. Microresonator soliton dual-comb spectroscopy. *Science* **354**, 600–603 (2016).

[12] Dell'Olio, F., Tatoli, T., Ciminelli, C. & Armenise, M. Recent advances in miniaturized optical gyroscopes. *Journal of the European Optical Society - Rapid publications* **9** (2014).

[13] Li, J., Suh, M.-G. & Vahala, K. Microresonator Brillouin gyroscope. *to be published in Optica* (2017).

[14] DelHaye, P. *et al.* Optical frequency comb generation from a monolithic microresonator. *Nature* **450**, 1214–1217 (2007).

[15] Herr, T. *et al.* Temporal solitons in optical microresonators. *Nature Photonics* **8**, 145–152 (2014).

[16] Yi, X., Yang, Q.-F., Yang, K. Y., Suh, M.-G. & Vahala, K. Soliton frequency comb at microwave rates in a high-Q silica microresonator. *Optica* **2**, 1078–1085 (2015).

[17] Lee, H. *et al.* Chemically etched ultrahigh-Q wedge-resonator on a silicon chip. *Nature Photonics* **6**, 369–373 (2012).

[18] Kippenberg, T. J., Spillane, S. M. & Vahala, K. J. Kerr-nonlinearity optical parametric oscillation in an ultrahigh-Q toroid microcavity. *Physical Review Letters* **93**, 083904 (2004).

[19] Savchenkov, A. A. *et al.* Low threshold optical oscillations in a whispering gallery mode CaF_2 resonator. *Physical Review Letters* **93**, 243905 (2004).

[20] Spillane, S., Kippenberg, T. & Vahala, K. Ultralow-threshold Raman laser using a spherical dielectric microcavity. *Nature* **415**, 621–623 (2002).

[21] Aoki, T. *et al.* Observation of strong coupling between one atom and a monolithic microresonator. *Nature* **443**, 671–674 (2006).

[22] Armani, D., Kippenberg, T., Spillane, S. & Vahala, K. Ultra-high-Q toroid microcavity on a chip. *Nature* **421**, 925–928 (2003).

[23] Grudinin, I. S., Ilchenko, V. S. & Maleki, L. Ultrahigh optical Q factors of crystalline resonators in the linear regime. *Physical Review A* **74**, 063806 (2006).

[24] Levy, J. S. *et al.* CMOS-compatible multiple-wavelength oscillator for on-chip optical interconnects. *Nature photonics* **4**, 37–40 (2010).

[25] Moss, D. J., Morandotti, R., Gaeta, A. L. & Lipson, M. New CMOS-compatible platforms based on silicon nitride and hydex for nonlinear optics. *Nature Photonics* **7**, 597–607 (2013).

[26] Spencer, D. T., Bauters, J. F., Heck, M. J. & Bowers, J. E. Integrated waveguide coupled Si_3N_4 resonators in the ultrahigh-Q regime. *Optica* **1**, 153–157 (2014).

[27] Xuan, Y. *et al.* High-Q silicon nitride microresonators exhibiting low-power frequency comb initiation. *Optica* **3**, 1171–1180 (2016).

[28] Pfeiffer, M. H. *et al.* Photonic Damascene process for integrated high-Q microresonator based nonlinear photonics. *Optica* **3**, 20–25 (2016).

[29] Ji, X. *et al.* Breaking the loss limitation of on-chip high-confinement resonators. *arXiv preprint arXiv:1609.08699* (2016).

[30] Li, Q. *et al.* Stably accessing octave-spanning microresonator frequency combs in the soliton regime. *arXiv preprint arXiv:1611.09229* (2016).

[31] Pfeiffer, M. H. *et al.* Octave-spanning dissipative Kerr soliton frequency combs in Si_3N_4 microresonators. *arXiv preprint arXiv:1701.08594* (2017).

[32] Cai, M., Painter, O. & Vahala, K. J. Observation of critical coupling in a fiber taper to a silica-microsphere whispering-gallery mode system. *Physical Review Letters* **85**, 74–77 (2000).

[33] Spillane, S. M., Kippenberg, T. J., Painter, O. J. & J., V. K. Ideality in a fiber-taper-coupled microresonator system for application to cavity quantum electrodynamics. *Physical Review Letters* **91**, 043902 (2003).

[34] Jones, D. J. *et al.* Carrier-envelope phase control of femtosecond mode-locked lasers and direct optical frequency synthesis. *Science* **288**, 635 (2000).

[35] Li, J., Lee, H., Chen, T. & Vahala, K. J. Low-pump-power, low-phase-noise, and microwave to millimeter-wave repetition rate operation in microcombs. *Physical Review Letters* **109**, 233901 (2012).

[36] Almeida, V. R., Panepucci, R. R. & Lipson, M. Nanotaper for compact mode conversion. *Optics letters* **28**, 1302–1304 (2003).

[37] Lecaplain, C., Javerzac-Galy, C., Gorodetsky, M. & Kippenberg, T. Mid-infrared ultra-high-Q resonators based on fluoride crystalline materials. *Nature Communications* **7** (2016).

[38] Brasch, V. *et al.* Photonic chip-based optical frequency comb using soliton Cherenkov radiation. *Science* **351**, 357–360 (2016).

[39] Yi, X., Yang, Q.-F., Yang, K. Y. & Vahala, K. Active capture and stabilization of temporal solitons in microresonators. *Optics Letters* **41**, 2037–2040 (2016).